

Design of practicable phase-change metadevices for near-infrared absorber and modulator applications

Santiago García-Cuevas Carrillo,¹ Geoffrey R. Nash,¹ Hasan Hayat,¹ Martin J. Cryan,² Maciej Klemm,² Harish Bhaskaran,³ and C. David Wright^{1,*}

¹College of Engineering, Mathematics and Physical Sciences, University of Exeter, Exeter EX4 4QF, UK

²Department of Electrical and Electronic Engineering, University of Bristol, Bristol, BS8 1TH, UK

³Department of Materials, University of Oxford, Parks Road, Oxford OX1 3PH, UK

*David.Wright@exeter.ac.uk

Abstract: Phase-change chalcogenide alloys, such as Ge₂Sb₂Te₅ (GST), have very different optical properties in their amorphous and crystalline phases. The fact that such alloys can be switched, optically or electrically, between such phases rapidly and repeatedly means that they have much potential for applications as tunable photonic devices. Here we incorporate chalcogenide phase-change films into a metal-dielectric-metal metamaterial electromagnetic absorber structure and design absorbers and modulators for operation at technologically important near-infrared wavelengths, specifically 1550 nm. Our design not only exhibits excellent performance (e.g. a modulation depth of ~77% and an extinction ratio of ~20 dB) but also includes a suitable means for protecting the GST layer from environmental oxidation and is well-suited, as confirmed by electro-thermal and phase-transformation simulations, to in situ electrical switching. We also present a systematic study of design optimization, including the effects of expected manufacturing tolerances on device performance and, by means of a sensitivity analysis, identify the most critical design parameters.

Published by The Optical Society under the terms of the [Creative Commons Attribution 4.0 License](#). Further distribution of this work must maintain attribution to the author(s) and the published article's title, journal citation, and DOI.

OCIS codes: (160.3918) Metamaterials; (260.5740) Resonance.

References and links

1. Y. Avitzour, Y. Urzhumov, and G. Shvets, "Wide-angle infrared absorber based on a negative-index plasmonic metamaterial," *Phys. Rev. B* **79**(4), 045131 (2009).
2. T. Maier and H. Brueckl, "Multispectral microbolometers for the midinfrared," *Opt. Lett.* **35**(22), 3766–3768 (2010).
3. Y. Wang, T. Sun, T. Paudel, Y. Zhang, Z. Ren, and K. Kempa, "Metamaterial-plasmonic absorber structure for high efficiency amorphous silicon solar cells," *Nano Lett.* **12**(1), 440–445 (2012).
4. Y. Cui, Y. He, Y. Jin, F. Ding, L. Yang, Y. Ye, S. Zhong, Y. Lin, and S. He, "Plasmonic and metamaterial structures as electromagnetic absorbers," *Laser Photonics Rev.* **8**(4), 495–520 (2014).
5. N. Liu, M. Mesch, T. Weiss, M. Hentschel, and H. Giessen, "Infrared perfect absorber and its application as plasmonic sensor," *Nano Lett.* **10**(7), 2342–2348 (2010).
6. B. Gholipour, J. Zhang, K. F. MacDonald, D. W. Hewak, and N. I. Zheludev, "An all-optical, non-volatile, bidirectional, phase-change meta-switch," *Adv. Mater.* **25**(22), 3050–3054 (2013).
7. P. Anh Do, A. Hendaoui, E. Mortazy, M. Chaker, and A. Haché, "Vanadium dioxide spatial light modulator for applications beyond 1200nm," *Opt. Commun.* **288**, 23–26 (2013).
8. L. Zou, M. Cryan, and M. Klemm, "Phase change material based tunable reflectarray for free-space optical inter/intra chip interconnects," *Opt. Express* **22**(20), 24142–24148 (2014).
9. S. Raoux, F. Xiong, M. Wuttig, and E. Pop, "Phase change materials and phase change memory," *MRS Bull.* **39**(8), 703–710 (2014).
10. C. Rios, P. Hosseini, C. D. Wright, H. Bhaskaran, and W. H. P. Pernice, "On-chip photonic memory elements

- p>employing phase-change materials,”
- Adv. Mater.*
- 26**
- (9), 1372–1377 (2014).
11. P. Hosseini, C. D. Wright, and H. Bhaskaran, “An optoelectronic framework enabled by low-dimensional phase-change films,” *Nature* **511**(7508), 206–211 (2014).
 12. C. D. Wright, Y. Liu, K. I. Kohary, M. M. Aziz, and R. J. Hicken, “Arithmetic and biologically-inspired computing using phase-change materials,” *Adv. Mater.* **23**(30), 3408–3413 (2011).
 13. C. D. Wright, P. Hosseini, and J. A. V. Diodado, “Beyond von-Neumann computing with nanoscale phase-change memory devices,” *Adv. Funct. Mater.* **23**(18), 2248–2254 (2013).
 14. M. A. Kats, D. Sharma, J. Lin, P. Genevet, R. Blanchard, Z. Yang, M. M. Qazilbash, D. N. Basov, S. Ramanathan, and F. Capasso, “Ultra-thin perfect absorber employing a tunable phase change material,” *Appl. Phys. Lett.* **101**(22), 221101 (2012).
 15. S. Cuffe, D. Li, Y. Zhou, F. J. Wong, J. A. Kurvits, S. Ramanathan, and R. Zia, “Dynamic control of light emission faster than the lifetime limit using VO₂ phase-change,” *Nat. Commun.* **6**, 8636 (2015).
 16. T. Cao, C. Wei, R. E. Simpson, L. Zhang, and M. J. Cryan, “Rapid phase transition of a phase-change metamaterial perfect absorber,” *Opt. Mater. Express* **3**(8), 1101 (2013).
 17. T. Cao, C. W. Wei, R. E. Simpson, L. Zhang, and M. J. Cryan, “Broadband polarization-independent perfect absorber using a phase-change metamaterial at visible frequencies,” *Sci. Rep.* **4**, 3955 (2014).
 18. Y. G. Chen, T. S. Kao, B. Ng, X. Li, X. G. Luo, B. Luk’yanchuk, S. A. Maier, and M. H. Hong, “Hybrid phase-change plasmonic crystals for active tuning of lattice resonances,” *Opt. Express* **21**(11), 13691–13698 (2013).
 19. A. Tittl, A.-K. U. Michel, M. Schäferling, X. Yin, B. Gholipour, L. Cui, M. Wuttig, T. Taubner, F. Neubrech, and H. Giessen, “A switchable mid-infrared plasmonic perfect absorber with multispectral thermal imaging capability,” *Adv. Mater.* **27**(31), 4597–4603 (2015).
 20. G. W. Burr, M. J. Breitwisch, M. Franceschini, D. Garetto, K. Gopalakrishnan, B. Jackson, B. Kurdi, C. Lam, L. A. Lastras, A. Padilla, B. Rajendran, S. Raoux, and R. S. Shenoy, “Phase change memory technology,” *J. Vac. Sci. Technol. B* **28**(2), 223–262 (2010).
 21. N. Liu, H. Guo, L. Fu, S. Kaiser, H. Schweizer, and H. Giessen, “Plasmon hybridization in stacked cut-wire metamaterials,” *Adv. Mater.* **19**(21), 3628–3632 (2007).
 22. R. Alae, M. Albooyeh, M. Yazdi, N. Komjani, C. Simovski, F. Lederer, and C. Rockstuhl, “Magnetolectric coupling in nonidentical plasmonic nanoparticles: theory and applications,” *Phys. Rev. B* **91**(11), 115119 (2015).
 23. T. G. Kolda, R. M. Lewis, and V. Torczon, “Optimization by direct search: new perspectives on some classical and modern methods,” *Soc. Ind. Appl. Math.* **45**(3), 385–482 (2003).
 24. P. B. Johnson and R. W. Christy, “Optical constants of the noble metals,” *Phys. Rev. B* **6**(12), 4370–4379 (1972).
 25. A. D. Rakić, A. B. Djurišić, J. M. Elazar, and M. L. Majewski, “Optical properties of metallic films for vertical-cavity optoelectronic devices,” *Appl. Opt.* **37**(22), 5271–5283 (1998).
 26. G. V. Naik, J. Kim, and A. Boltasseva, “Oxides and nitrides as alternative plasmonic materials in the optical range,” *Opt. Mater. Express* **1**(6), 1090 (2011).
 27. F. Lai, L. Lin, R. Gai, Y. Lin, and Z. Huang, “Determination of optical constants and thicknesses of In₂O₃:Sn films from transmittance data,” *Thin Solid Films* **515**(18), 7387–7392 (2007).
 28. L. Lin, F. Lai, Y. Qu, R. Gai, and Z. Huang, “Influence of annealing in N₂ on the properties of In₂O₃:Sn thin films prepared by direct current magnetron sputtering,” *Mater. Sci. Eng. B* **138**, 166–171 (2007).
 29. F. Yi, E. Shim, A. Y. Zhu, H. Zhu, J. C. Reed, and E. Cubukcu, “Voltage tuning of plasmonic absorbers by indium tin oxide,” *Appl. Phys. Lett.* **102**(22), 221102 (2013).
 30. K. Shportko, S. Kremers, M. Woda, D. Lencer, J. Robertson, and M. Wuttig, “Resonant bonding in crystalline phase-change materials,” *Nat. Mater.* **7**(8), 653–658 (2008).
 31. J. A. Vázquez Diodado, P. Ashwin, K. I. Kohary, and C. D. Wright, “Threshold switching via electric field induced crystallization in phase-change memory devices,” *Appl. Phys. Lett.* **100**(25), 253105 (2012).
 32. P. Ashwin, B. S. V. Patnaik, and C. D. Wright, “Fast simulation of phase-change processes in chalcogenide alloys using a Gillespie-type cellular automata approach,” *J. Appl. Phys.* **104**(8), 084901 (2008).
 33. L. Y. Mario, S. Darmawan, and M. K. Chin, “Asymmetric Fano resonance and bistability for high extinction ratio, large modulation depth, and low power switching,” *Opt. Express* **14**(26), 12770–12781 (2006).
 34. G. T. Reed, G. Mashanovich, F. Y. Gardes, and D. J. Thomson, “Silicon optical modulators,” *Nat. Photonics* **4**(8), 518–526 (2010).

1. Introduction

Thin-film electromagnetic absorbers have a number of important applications in the infrared and visible part of the spectrum including infrared detection [1,2], solar energy harvesting [3,4] and refractive index sensing [5]. Similarly, thin-film light modulating devices are much in demand for optical communications, optical signal processing and spatial light modulator applications [6–8]. In this paper we design novel near-infrared forms of thin-film electromagnetic absorbers and modulators that combine metamaterial arrays with switchable chalcogenide alloy films. Chalcogenide phase-change alloys, such as (Ge₂Sb₂Te₅) (GST), are

materials whose electrical and optical properties differ very considerably between their amorphous and crystalline phases and which can be (electrically or optically) switched between such phases quickly and repeatedly. This has led to their application in a variety of areas, in particular for non-volatile memory devices [9,10], but also more recently for the provision of solid-state and flexible displays [11] and for the realization of new approaches to computing [12,13]. By including such phase-change materials into a plasmonic (metamaterial) resonator structure, the optical properties in the environment of the resonator can be modified according to the phase-state of the chalcogenide material, so yielding an active device suited to, for example, a tunable absorber or an electrically or optically controlled (switched) modulator. A typical modulator structure is shown schematically in Fig. 1(a), consisting of a 4-layer arrangement comprising a bottom metal layer, the chalcogenide phase-change layer, an ITO layer and a patterned top metal layer (here patterned into strips); on switching of the state (from amorphous to crystalline or vice-versa) of the phase-change layer, the intensity of light reflected from the structure is modulated. Note that while here we concentrate on the use of $\text{Ge}_2\text{Sb}_2\text{Te}_5$ as the phase-change medium (due to its attractive and well-understood properties and behavior), other phase-change materials could of course be used. Indeed other common chalcogenides, such as AgInSbTe (AIST), have broadly similar optical properties to $\text{Ge}_2\text{Sb}_2\text{Te}_5$ and could (with appropriate structure optimizations) be incorporated into the designs we present below as an alternative to GST. One might also use non-chalcogenide phase-switching materials, in particular VO_2 which is known to have a large refractive index change when heated to switch it from its insulating to metal phase [14,15]. However, the phase-transition in VO_2 is volatile (the material returning to its insulating phase on cooling), whereas in GST (and AIST etc.) it is non-volatile, meaning that any particular (amorphous or crystalline) state can be maintained without the requirement for input power – a particularly attractive feature in terms of device performance.

Previous work on GST-metamaterial structures has concentrated on the mid-infrared part of the spectrum, with applications such as improved energy absorption in optical memories [16,17] or tunable photonic crystals [18], but the near-infrared (NIR) region has remained largely under-explored, due perhaps to the fact that the optical losses in GST start to rise appreciably in that region. However, operation in the NIR region is important since the most commonly used wavelengths for optical communications and optical signal processing lie in this region, specifically between 1530 nm to 1565 nm for the conventional C-band. Furthermore, in previous studies, the requirement to protect the active chalcogenide alloy layer from the effects of oxidation appears to have been largely ignored. The properties of chalcogenide alloy thin films are known to deteriorate rapidly on exposure to air and so for practicable absorber or modulator designs the chalcogenide phase-change layer should be encapsulated by a protective layer that, to maintain optical access and to allow for the possibility for electrical switching, should ideally be both optically transparent and electrically conductive [11]. We here use indium tin oxide (ITO) to provide such a layer. In addition, in terms of the choice of the composition of the (top and bottom) metal layers, gold and silver are usually the metals of choice in the literature, since they have excellent plasmonic behavior. However, Ag is particularly diffusive, especially at the high temperatures experienced during the switching of the phase-change layer and is thus best avoided. Aluminum has also been suggested as an alternative for the metal layers [19]. But, the melting point of aluminum (at $\sim 660^\circ\text{C}$) is relatively low, and in particular is very close to that ($\sim 620^\circ\text{C}$) of the GST alloy we use here. Since to amorphize the GST layer we need to heat it to above its melting temperature (and then cool it quickly), there is a danger that the top Al metal layer in particular would also melt (and, without any encapsulation, distort), and so the use of Al, at least with $\text{Ge}_2\text{Sb}_2\text{Te}_5$, is also problematic. In cases where electrical switching of the phase-change layer is the intended approach, the choice for the metal layers should also be guided by electrical as well as optical considerations. Thus, for effective

electrical switching of GST-based structures we might draw on the experience of phase-change memory developments, where tungsten (W) and titanium nitride (TiN) are the electrode materials of choice [20]. In this work therefore, and in a contrast to the usual practice, we have explored the use of various materials (including Au, Al, W, Ti, TiN) for both the top and bottom metal layers. We also include a full electro-thermal and phase-transformation simulation of electrical switching in our absorber/modulator structures, confirming their suitability for such a mode of operation.

The plasmonic resonator structure designed in this work is thus of the form shown in Fig. 1 and comprises a top metal layer (shown as Au in the figure) patterned into strips (or squares for a polarization insensitive design – see §3.1), a 'dielectric' space, consisting of both the indium tin oxide (ITO) layer (for environmental protection) and the phase-switchable GST layer, and a (thick) metallic bottom layer. The incident light induces a plasmonic resonance in the top patterned metal layer, essentially generating an oscillating in-plane electric dipole [21,22]. This dipole couples to the bottom metal layer, with the strength of the coupling dependent on the phase-state of the GST layer. With the GST in the amorphous (low k , low absorption) state, there is strong coupling of the electric field between the top and bottom metal layers, resulting in an anti-symmetric coupled state (the E-field in the bottom metal layer being anti-parallel to that in the top) and the generation of an oscillating magnetic dipole oriented orthogonally to the electric dipoles. Under such conditions, i.e. in the case of coupled resonators with both electric and magnetic dipoles, Alaei et al. [22] showed that by correct scaling of the dimensions of the top and bottom metal layers near perfect absorption can be achieved (and essentially our design approach finds such correct scaling conditions). However, with the GST in the crystalline (high k , high absorption) state, the coupling strength (for the E-field) between the top and bottom metal layers is very significantly reduced such that the induced magnetic dipole is very weak (effectively zero). Under these conditions the electric dipoles of the top metal layer effectively re-radiate the incoming light, leading to a high reflectance.

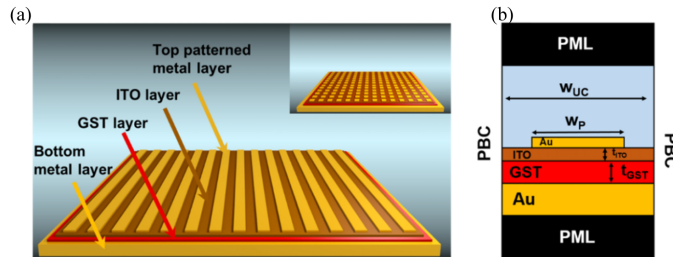


Fig. 1. (a) Schematic of a thin-film phase-change metamaterial absorber/modulator (inset shows the top metal layer patterned into squares for a polarization insensitive design). (b) 2D cross section of the phase-change NIR absorber/modulator studied here and having a bottom metal layer (here shown as Au) of fixed thickness 80 nm, a top metal layer (again here shown as Au) of fixed thickness 30 nm (both gold layers have a 5 nm Ti adhesion layer not included in the figure for clarity) patterned into strips of variable width w_p , and GST and ITO layers with variable thicknesses t_{GST} and t_{ITO} respectively. For the design simulations a unit cell of width w_{UC} is used, with periodic boundary conditions (PBC) of Bloch-Floquet type assumed and a perfect matching layer (PML) placed at the top and bottom of the structure.

To reiterate, the aim of this work is to design phase-change-based electromagnetic absorber and modulator devices for use in the NIR, based on the resonator structure shown in Fig. 1, taking proper account, by way of protective layers for the GST and the choice of the metal layers, issues of practicability, specifically environmental stability/resistance to oxidation and suitability for electrical switching of the phase-change layer. We also take into account, for the first time and via a detailed optimization and tolerance analysis, the effects of manufacturing tolerances (e.g. deposition tolerances affecting the thickness of individual

layers, lithographic tolerances affecting the dimensions of the patterned areas) on key device performance parameters and we identify the most critical tolerances by means of a sensitivity analysis.

2. Materials and methods

The reflectance properties of our phase-change metamaterial absorber/modulator were calculated by solving the wave equation for the electric field over the entire unit cell shown in Fig. 1(b), using finite-element (FE) techniques within the commercial software environment COMSOL Multiphysics[®]. By solving the wave equation for the electric field in a stationary analysis of the unit cell under periodic boundary conditions and assuming a time-harmonic excitation field, it is possible to calculate the scattering parameter matrix and hence the fraction of energy that it is reflected, transmitted and absorbed. At the top and the bottom of the unit cell we assumed a perfect matched layer to simulate the conditions of free-space. Input parameters to the simulation include the thicknesses and optical constants of each layer (electric permittivity/complex refractive index), along with the width of the strips (or size of squares) in the top metal layer and the size of the unit cell. For the case of the top metal layer patterned into strips, a 2D solution is sufficient, whereas for the top layer patterned into squares, a full 3D solution is required. We assume normal incidence and for the 2D case the incident polarization is assumed to be in the plane of the film and perpendicular to the direction of the patterned metal strips. For the case of the top metal layer patterned into squares, the polarization can be in any direction, but still in the plane of the film.

An optimization and tolerance analysis of the design was also carried out (see §3.2), for which a pattern search algorithm [23] in the Matlab[®] optimization toolbox and LiveLink for Matlab were used.

The values for the refractive index of the various metals explored were taken from the literature, specifically values for gold are taken from Johnson and Christy [24]; values for Al, W and Ti from [25]; and for TiN from [26]. The optical and electrical constants of ITO depend on several factors, in particular on the process conditions during deposition, as well as on any annealing regime used post-deposition. While post-deposition annealing generally increases the electrical conductivity of ITO, it also increases the extinction coefficient in the NIR region and therefore the optical losses, potentially leading to a deterioration of the performance of absorber/modulator designs investigated here. However, according to [27,28], the optical losses of ITO remain low in the NIR as long as there is no annealing after deposition; thus, here we assume ITO has the properties of un-annealed material and the relevant optical constants have been taken from published ellipsometry measurements in [29]. The optical constants of GST in both the amorphous and crystalline phase were taken from commonly-used values, as detailed in [30].

With regard to the modelling of the electrical phase-switching behavior of GST, we use a combined electro-thermal simulation tool that simultaneously solves the Laplace and heat-diffusion equation in order to determine the temperature distribution throughout the structure at each simulation time step. This temperature distribution feeds into a Gillespie cellular automata (GCA) model that solves for the phase (i.e. determines if each cell in the simulation is in the melted, amorphous or crystalline state) using a rate-equation approach. Our electro-thermal-GCA model has proved to be capable of realistic simulations of both blanket thin-film behavior and phase-change device operation, and has been described in detail in previous works [13,31,32] to which the reader is referred for further information.

3. Results and discussion

3.1 Optimized NIR modulator design

We now turn our attention to the design of an optical modulator working in reflection (as shown schematically in Fig. 1(a) and having the structure of Fig. 1(b)) and tuned to the

technologically important wavelength of 1550 nm. By switching the GST layer between its amorphous and crystalline phases (a process that can be done optically or electrically), we can control its absorption/reflection properties, so providing for an active, switchable, thin-film modulator.

First, we need to consider appropriate figures of merit with which to measure the performance of a particular modulator design. Here we use in particular the modulation depth (*MD*) which is defined [33] as the difference between the maximum reflected power P_{max} (which here will occur when the GST layer is in the crystalline phase) and the minimum reflected power P_{min} (here when the GST will be in the amorphous phase), normalized by the incident power (P_{inc}), i.e.

$$MD = \frac{P_{max} - P_{min}}{P_{inc}} = R_{cr} - R_{am} \quad (1)$$

where R_{cr} and R_{am} are the reflectance of the modulator when the GST layer is in the crystalline and amorphous phases respectively. Another commonly used figure of merit is the extinction ratio (*ER*), which is usually defined (for reflection modulators) in terms of the logarithm of the ratio of the maximum to the minimum reflected power, i.e.

$$ER = -10 \log_{10} \frac{P_{max}}{P_{min}} = -10 \log_{10} \frac{R_{cr}}{R_{am}} \quad (2)$$

A large modulation depth and high extinction ratio are always desirable, with *ER* values better than -7 dB being a typical design target for practicable modulators [34], although for some applications, such as short-reach optical interconnects, an *ER* of around -5 dB is often considered to be sufficient [6].

Using the Matlab[®] pattern search algorithm, the structure of Fig. 1 was optimized in terms of the maximum modulation depth. We began by assuming both the top and bottom metal layers were made of gold. The dimensions of the unit cell (w_{UC}), the top Au layer strip width (w_p), the thickness of the ITO layer (t_{ITO}) and the thickness of the GST layer itself (t_{GST}) were all allowed to vary, while the thicknesses of the top and bottom Au layers were fixed at 30 nm and 80 nm respectively (with an additional 5 nm Ti adhesion layer). The dimensions that give an optimized (maximum) *MD* at 1550 nm were found to be $w_{UC} = 493.3$ nm, $w_p = 333.8$ nm, $t_{GST} = 64.1$ nm and $t_{ITO} = 5.0$ nm. Note that the optimum thickness of the ITO layer, t_{ITO} , returned by the optimization algorithm is coincident with the lowest value we allowed in the search (this lower limit having been chosen to ensure reliable deposition of the continuous layer of ITO needed for the desired environmental protection of the GST layer). The reflectance of this optimized modulator, with the GST layer in both the crystalline and the amorphous states, is shown in Fig. 2(a), while the extinction ratio is shown in Fig. 2(b).

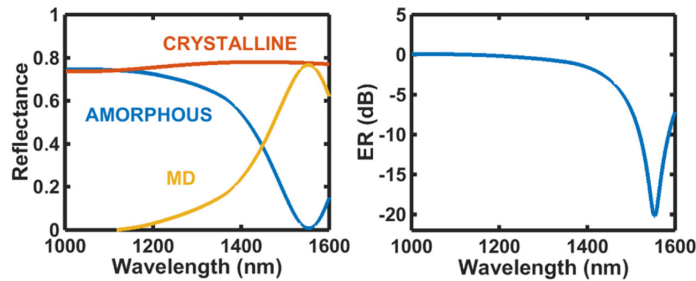


Fig. 2. (a) Simulated reflectance spectrum for the design in Fig. 1 with Au top and bottom metal layers and with the phase-change layer in both the crystalline and amorphous states. The chalcogenide phase-change layer here is $\text{Ge}_2\text{Sb}_2\text{Te}_5$ (GST) and the design was optimized for maximum modulation depth (MD) at 1550 nm. Also shown (b) is the extinction ratio.

It is clear from Fig. 2 that the optimally designed modulator should provide excellent performance, with optimum values for MD and ER being very high, at 0.767 and -19.8 dB respectively for the target wavelength of 1550 nm. (Note that, as discussed in §1, if we were to replace the GST layer with AIST we can still obtain very good performance, specifically here a MD of 0.645 and an ER of -14.7 dB with, in this case, $w_{UC} = 657.5$ nm, $w_p = 324.7$ nm, $t_{AIST} = 53.7$ nm and $t_{ITO} = 5.0$ nm)

In terms of the polarization of the incident radiation, as pointed out in the introduction, the patterning of the top metal layer into strips or squares will result in, respectively, a polarization dependent or independent operation (assuming normal incidence). This is confirmed in Fig. 3, where we compare the performance of both types of modulators, i.e. top layer patterned into (a) strips and (b) squares, for various incident polarizations.

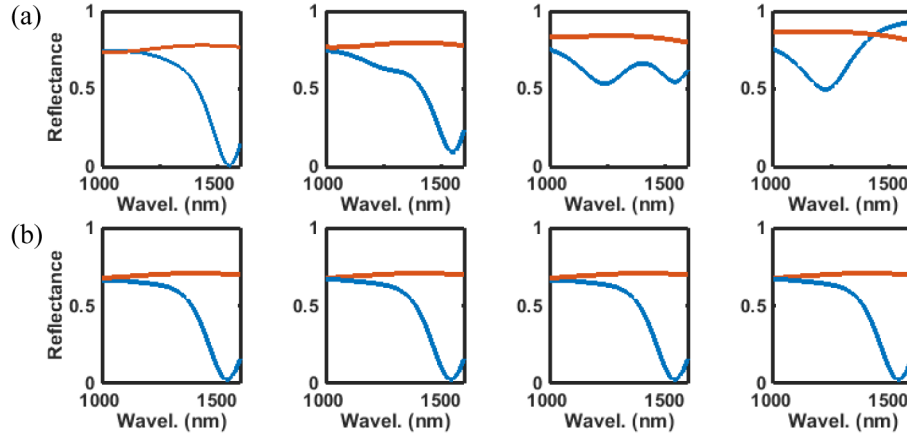


Fig. 3. The reflectance spectrum of the modulator for different incident polarizations and with the top layer patterned into (a) strips (of the same width and spacing as in Fig. 2) and (b) squares (with sides of length equal to the width of the strips in Fig. 2). The polarization angles in each case are, going from left to right, 0 degrees (electric field perpendicular to the strips), 30 degrees, 60 degrees and 90 degrees (electric field parallel to strips). It is clear that in the case of the top metal layer patterned into squares the design is polarization independent (for normal incidence). In all cases red lines show results for the GST layer in the crystalline phase and blue the amorphous phase.

3.2 Effect of choice of metal layers on modulator performance

As discussed in §2 above, we also investigated the effect on modulator optical performance of the choice of different materials for the top and bottom metal layers, rather than simply using the *de facto* choice, from a plasmonic perspective, of gold. Specifically we compared the use of Au against that of Al, W and TiN. We found that we could obtain excellent absorber/modulator optical performance when Al was used for the top and bottom layers, as shown in Fig. 4(a) and as also reported, for the MIR range, in the literature [19] (but note our previous comments regarding the possible unsuitability of Al due to its low melting point). For W and TiN layers (typical electrode materials in phase-change memory devices) we found that excellent absorber/modulator performance could be obtained if W and TiN were used for the top metal layer only, but not if used for the top and bottom layers, as shown in Fig. 4(b) and 4(c). This can be explained if we consider the absorber as a periodic structure capable of adding momentum to the incoming radiation in the horizontal direction (as we explained in §1), a process that requires the bottom metal layer to be one that exhibits excellent plasma behavior, such as Au (or Al), in order to obtain near zero reflectance with the phase-change layer in the amorphous phase. The results of Fig. 4 certainly show that, at least from an optical perspective, the choice of metals available for use in these phase-change metadvice structures is much wider than the usual plasmonic favorites of Au or Ag.

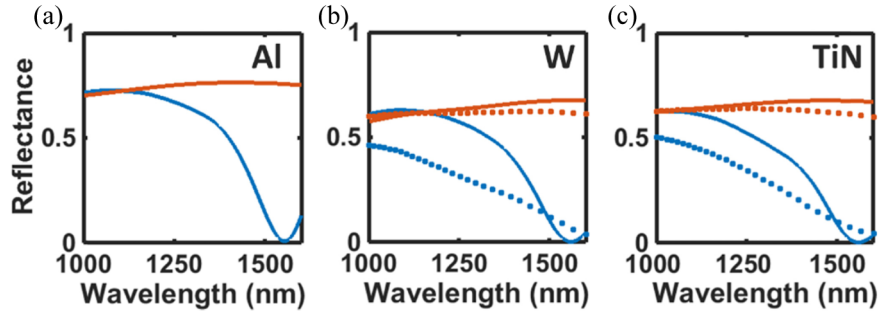


Fig. 4. The reflectance spectrum for optimized (in terms of MD at 1550 nm) phase-change modulators of the form of Fig. 1 but with (a) Al top and bottom metal layers, (b) (i) W top and bottom layers (dotted lines) and (ii) W top and Au bottom layers (solid lines) and (c) (i) TiN top and bottom layers (dotted lines) and (ii) TiN top and Au bottom layers (solid lines). In all cases red lines show results for the GST layer in the crystalline phase and blue the amorphous phase.

3.3 Sensitivity analysis

A drawback of the optimization methods used in the previous section is that the optimal solution returns very precise values of the key design parameters for the modulator, i.e. the ITO and GST layer thicknesses, the width of the strips in the top metal layer and the unit cell dimensions. Achieving such precise values using a practicable manufacturing method is very unlikely, at least with any degree of cost effectiveness. Indeed, using common deposition methods, such as magnetron sputtering, for the various layers in the stack one might expect a thickness tolerance of perhaps ± 1 nm at best. Standard lithography techniques for the patterning of the top layer, such as e-beam lithography, would also be expected to have similar, if not even larger, tolerances. It is therefore important, from a fabrication and manufacturing perspective, to understand how the performance of the optimally designed modulator is affected (deteriorated) by such fabrication tolerances.

We here address this problem via a sensitivity analysis, simulating the performance of the modulator over a region of parameter space defined by the realistic tolerances in the thicknesses of the GST and ITO layers and in the size (width) of the strips in the top metal layer. Specifically we assumed normally-distributed layer thicknesses (t_{GST} and t_{ITO}) with $\sigma = 0.5$ nm, along with normally-distributed strip width and unit-cell dimensions (w_P and w_{UC}) with $\sigma = 7.5$ nm, and calculated the modulation depth, MD , for a total of over 2000 points randomly distributed in the parameter space encompassed by these variations. Results, for the absorber/modulator of Fig. 2 (and with Au top and bottom metal layers) are given in the scatter plots of Fig. 5 where we show the MD for all points in the parameter space lying within $\pm 2\sigma$ of the mean values of t_{GST} , t_{ITO} , w_P and w_{UC} . It can be seen that the parameters having most effect on modulator performance (at least on the modulation depth) are the thickness of the ITO layer and the width of the strips in the top metal layer (in particular the former). From all the produced solutions we can calculate the mean and the standard deviation to have an idea of how these solutions (for the modulation depth) are distributed with respect the optimum value which, we recall, was $MD = 0.767$ (as in Fig. 2(a)). Thus, for the solutions shown in Fig. 5, the mean value of the modulation depth is 0.760 with a standard deviation of $\sigma_{MD} = 0.008$. The fact that the mean is so close to the optimal value and the standard deviation is relatively small tells us that our design is indeed stable to the tolerances in layer thicknesses and lithographic patterning expected to arise as a result of typical fabrication/manufacturing processes.

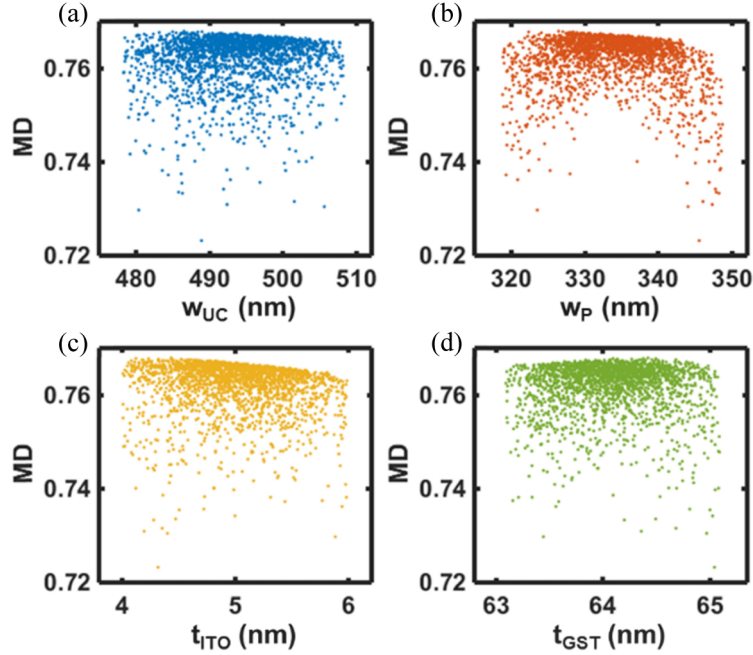


Fig. 5. Scatter plot showing the variation of the phase-change metadvice modulation depth (MD) when typical manufacturing tolerances are included in the design and for the key parameters of (a) unit cell width w_{UC} , (b) width of top metal strips w_P , (c) thickness of the ITO layer, t_{ITO} and (d) thickness of the GST layer, t_{GST} .

3.5 Electrical switching

A key feature of phase-change metadvice is of course the ability to dynamically change/tune/reconfigure the device response by switching the phase-change layer between the amorphous and crystalline states (or indeed to some intermediate mixed phase). It is crucial therefore that devices be designed from the outset to enable such switching to occur, either by electrical or optical means. Amorphization is conventionally achieved by heating the phase-change layer above its melting point ($\sim 620^\circ\text{C}$ in $\text{Ge}_2\text{Sb}_2\text{Te}_3$) followed by rapid cooling (the cooling rate needs to be many tens of degrees per nanosecond to prevent recrystallization). Crystallization is achieved by heating to a temperature above the crystallization temperature, but below that of melting. Any device structure needs therefore to be designed to enable the phase-change layer to be heated, by appropriate excitations, to the requisite temperatures and also to allow sufficiently fast cooling for the amorphous phase to form.

Phase-change metadvice so far reported in the literature have generally been switched ex-situ using fast, high-power external lasers, or simply by carrying out thermal annealing in an oven to induce a one-way transition from the amorphous to crystalline phase (due to the fast cooling requirements, oven annealing cannot be used to form the amorphous phase) [6,19]. For real-world applications however, some form of in situ switching of the phase-change layer would be most attractive. In our case, this might be achieved by dividing the absorber/modulator structure of the form shown in Fig. 1 into an arrangement of pixels, each of which could be separately excited electrically in order to switch the phase-change layer (for example, in the case of a modulator with the topmost metal layer patterned into strips, one might also pattern the bottom metal layer into (orthogonal) strips, yielding a structure electrically similar to the commonly used cross-bar memory devices in which individual

‘cells’ are addressed by appropriate excitations being placed on the relevant intersecting strips - the so-called ‘bit’ and ‘word’ lines in memory device terminology [11,20]).

We have thus simulated electrical switching by assuming each pixel is represented by the unit-cell of the form shown in Fig. 1(b) (with dimensions optimized for maximum modulation depth as in Fig. 2) and applied appropriate electrical pulses between the top and bottom metal layers of the structure in order to determine whether amorphization and crystallization of the phase-change layer can indeed be achieved using in situ electrical excitation. Typical results are shown in Fig. 6, here for the case of Au top and bottom metal layers (though similar results were obtained for Al, W and TiN) using a 2.4 V, 50ns (15/5 ns rise/fall time) amorphization, or so-called RESET, pulse and a 1.4 V, 100 ns (30 ns rise/fall time) crystallization, or so-called SET, pulse. In Fig. 6(a) we show the temperature distributions throughout the unit-cell at the time (during the excitation pulse) at which the maximum temperature occurs for both RESET and SET pulses. During the RESET pulse the maximum temperature does indeed exceed the melting point of GST (620 °C or 893 K), and the temperature distribution is relatively uniform throughout the GST layer. We also note that the temperature experienced by the top metal layer is also relatively high in this case (~980 K), precluding the use of aluminum (melting point ~933 K) for the top layer, as discussed in §1 (replacing the top Au layer with Al in the simulations shown in Fig. 6(a) did not significantly affect the maximum temperature reached). During the SET pulse, the maximum temperature experienced by the GST layer is in the region of 720 K or 447 °C, a typical value required to ensure rapid (on the order of tens of nanoseconds) crystallization of GST [31]. In Fig. 6(b) we show the starting and finishing phase states of the GST layer (calculated using our Gillespie Cellular Automata approach –see §2 and [32]) after a sequence of RESET/SET/RESET pulses: the GST layer starts in the fully crystalline state (shown brown in Fig. 6(b)); after the application of a first RESET pulse the GST layer is fully amorphized (shown blue in Fig. 6(b)); after the application of the SET pulse the GST layer is fully re-crystallized (into a number of crystallites, as shown by the different colors in Fig. 6(b)); finally, after the receipt of a second RESET pulse the GST layer is fully re-amorphized.

Thus it would appear, at least from a simulation perspective (and for the material properties shown in Table 1), that phase-change metadevices of the form described in this paper would indeed be suited to in situ electrical switching of the phase-change layer, so providing a readily active/tunable/reconfigurable photonic response. (We also note that, to avoid any possible concerns of gold diffusion from the bottom metal layer into the GST layer [6], an additional ITO layer can be inserted on top of the bottom Au layer without any detrimental effects, in an appropriately optimized structure, on the overall electrical or optical performance).

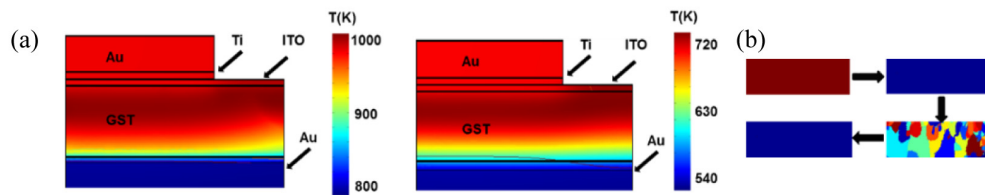


Fig. 6. (a) Simulated temperature distributions in the structure of Fig. 1(b) for the case of electrical excitation (assuming an electrically pixelated structure with pixel size equal to the unit-cell size) for (left) a RESET (amorphization) pulse of 2.4V/50 ns and (right) a SET (crystallization) pulse of 1.4V/100ns respectively. (b) The starting and finishing phase-states of the GST layer after a sequence of RESET/SET/RESET electrical excitations: the GST layer starts in the fully crystalline state (shown brown); after the application of a first RESET pulse the GST layer is fully amorphized (shown blue); after the application of a SET pulse the GST layer is fully re-crystallized (into a number of crystallites, as shown by the different colors); finally, after the receipt of a second RESET pulse the GST layer is fully re-amorphized.

Table 1. Materials parameters used in phase-switching simulations of Fig. 6

Material	Thermal Conductivity (W/mK)	Heat Capacity (J/kg.K)	Electrical Conductivity ($\Omega^{-1}\text{m}^{-1}$)
Au	310	129	44×10^6
ITO	11	340	8.3×10^3
Ti	7.5	710	7.4×10^5
GST (Amorphous)	0.2	210	See (A)
GST (Crystalline)	0.58	210	See (A)
Si (Substrate)	149	720	100

(A) C D Wright et al., *IEEE Transactions on Nanotechnology* 5, 1 (2006)

4. Conclusions

In summary, we have shown that it is feasible to design chalcogenide-based phase-change metadevices for absorber and modulator applications and suited to operation in the technologically important near-infrared range of the spectrum, specifically here 1550 nm. Furthermore, we have shown that it is possible to design such devices using a practicable approach providing environmental stability by incorporating an ITO layer to protect the GST from oxidation while still allowing both optical and electrical access. Moreover, we have shown how the optimization of such designs can be carried out while taking proper account of likely fabrication and manufacturing tolerances and allowing for the use of a variety of metal layers rather than just relying on the standard ‘plasmonic choices’ of gold or silver. Finally, we have confirmed by simulation that suitably pixelated versions of such phase-change metadevices should be capable of being switched by in situ electrical excitation using pulsing regimes similar to those used in phase-change memory device applications.

Acknowledgments

CDW and HB acknowledge funding by way of EPSRC grants EP/M015173/1 and EP/M015130/1. SG-CC acknowledges funding from the EPSRC Centre for Doctoral Training in Metamaterials, grant number EP/L015331/1. CDW and SG-CG would like to acknowledge helpful discussions with Dr A Alexeev (University of Exeter) regarding the plasmonic behavior of our device design.